
Data-efficient Hindsight Off-policy Option Learning

Markus Wulfmeier, Dushyant Rao, Roland Hafner, Thomas Lampe, Abbas Abdolmaleki,
Tim Hertweck, Michael Neunert, Dhruva Tirumala, Noah Siegel,
Nicolas Heess, Martin Riedmiller

DeepMind, London, UK
mwulfmeier@google.com

Abstract

Solutions to most complex tasks can be decomposed into simpler, intermediate skills, reusable across wider ranges of problems. We follow this concept and introduce Hindsight Off-policy Options (HO2), a new algorithm for efficient and robust option learning. The algorithm relies on critic-weighted maximum likelihood estimation and an efficient dynamic programming inference procedure over off-policy trajectories. We can backpropagate through the inference procedure through time and the policy components for every time-step, making it possible to train all component’s parameters off-policy, independently of the data-generating behavior policy. Experimentally, we demonstrate that HO2 outperforms competitive baselines and solves demanding robot stacking and ball-in-cup tasks from raw pixel inputs in simulation. We further compare autoregressive option policies with simple mixture policies, providing insights into the relative impact of two types of abstractions common in the options framework: action abstraction and temporal abstraction. Finally, we illustrate challenges caused by stale data in off-policy options learning and provide effective solutions.

1 Introduction

Deep reinforcement learning has had considerable successes in recent years [21, 32, 38]. However, applications in domains with limited or expensive data have so far been rare. To address this challenge, data efficiency can be improved through additional structure imposed on the solution space available to an RL agent, reducing the information that needs to be extracted from data.

The options framework [22, 34] formalizes the intuition that solutions to many tasks can be composed from reusable behaviors. Options introduce a form of action abstraction, that can reduce the complexity and frequency of action choice between sub-behaviours. Especially in multi-task domains, this abstraction can accelerate learning by enabling a high-level controller to compose solutions from a set of cross-task, domain-dependent skills. The hierarchical control scheme imposed by the options framework can provide conceptual advantages but may also introduce additional complexities, including possible degenerate cases [11, 22], trade-offs regarding option length [12], and additional stochasticity. These can increase the difficulty of the problem, especially in an off-policy setting [24].

With Hindsight Off-policy Options (HO2), we present a method for data-efficient, off-policy learning of options, for robotics and other continuous action-space domains. The algorithm builds on advances in off-policy policy optimization [2, 39] and combines these with an efficient dynamic programming procedure to infer option probabilities along trajectories and update all policy parts via backpropagation (conceptually related to [25, 31, 33]). The result is an actor-critic algorithm that computes policy updates via critic-weighted maximum-likelihood. To stabilize policy updates, HO2 uses adaptive trust-region constraints, demonstrating the importance of robust policy optimization for hierarchical reinforcement learning (HRL) in line with recent work [40]. Rather than conditioning on executed options, the algorithm treats these as unobserved variables, computes the marginalized likelihood, and enables exact gradient computation without relying on Monte Carlo approximation or continuous

relaxation [18]. Intuitively, the approach can be understood as inferring option and action probabilities for off-policy trajectories in hindsight and maximizing the likelihood of good actions and options by backpropagating through the inference procedure. It also allows us to impose hard constraints on the option termination frequency thereby regularizing the learned solution without introducing additional loss terms. The algorithm additionally generates rewards for all tasks in hindsight for trajectories in multi-task domains. This makes it possible to compute updates from data for all policy components independent of the option and task which was used to generate data.

We evaluate the algorithm in both single and multi-task domains. In single-task domains we demonstrate that our approach outperforms several previously proposed option learning schemes. Our evaluation in multi-task domains indicates the benefits of options as domain-specific, task-independent skills in both parallel and sequential transfer settings. We find that HO2 considerably outperforms recent work and is able to solve complex 3D robot manipulation tasks from raw pixel inputs. To better understand the relevant properties of our approach we perform several ablations and investigate the impact of learning options in an off-policy context. Most importantly, we compare option policies, with and without temporal regularization, to simple mixture policies which allows us to disentangle the benefits of action abstraction via shared components from those arising from temporal abstraction.

2 Method

We consider a reinforcement learning setting with an agent operating in a Markov Decision Process (MDP) consisting of the state space \mathcal{S} , the action space \mathcal{A} , and the transition probability $p(s_{t+1}|s_t, a_t)$ of reaching state s_{t+1} from state s_t when executing action a_t . The actions a_t are drawn from the agent’s policy $\pi(a_t|x_t)$, where x_t can either refer to the current state s_t of the agent or, in order to model dependencies on the previous steps, the trajectory until the current step, $h_t = \{s_t, a_{t-1}, s_{t-1}, \dots, s_0, a_0\}$. Jointly, the transition dynamics and policy induce the marginal state visitation distribution $p(s_t)$. The discount factor γ together with the reward $r_t = r(s_t, a_t)$ gives rise to the expected return, which the agent aims to maximize: $J(\pi) = \mathbb{E}_{p(s_t), \pi(a_t, s_t)} \left[\sum_{t=0}^{\infty} \gamma^t r_t \right]$.

We start by describing mixture policies as an intermediate between flat policies and the option framework (see Figure 1), which introduce a type of action abstraction via multiple low-level policies. Subsequently, we extend the description to option policies which add the modelling of temporal abstraction via autoregressive option transitions. To bridge between mixture and option policy models, we will use the terms component and option interchangeably. The next paragraphs focus on computing likelihoods of actions and options or components under a policy which are required to define the critic-weighted maximum likelihood algorithm for improvement of hierarchical policies.

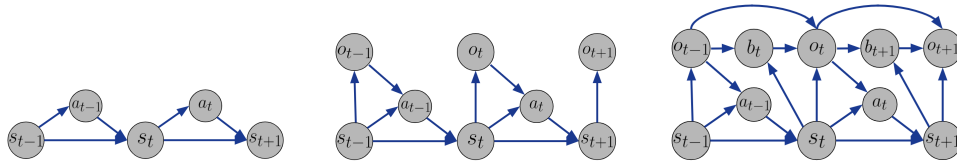


Figure 1: Graphical model for flat policy (left), mixture policy (middle) - introducing a type of action abstraction, and option policy (right) - adding temporal abstraction via autoregressive options.

Likelihood under Mixture Policies A mixture policy can be seen as a simplification of the options framework without initiation or termination condition and resampling of options after every step (i.e. there is no direct conditioning between the options of time-step t and $t + 1$ in Figure 1). The joint probability of action and option under the mixture is given as:

$$\pi_{\theta}(a_t, o_t|s_t) = \pi^L(a_t|s_t, o_t) \pi^H(o_t|s_t), \text{ with } \pi^H(o_t|s_t) = \pi^C(o_t|s_t), \quad (1)$$

where π^H and π^L respectively represent high-level policy (which for the mixture is equal to a Categorical distribution π^C) and low-level policy (components of the resulting mixture distribution), and o is the index of the sub-policy or mixture component.

Likelihood under Option Policies We will follow the *call-and-return* option model [34], defining an option as a triple $(I(s_t, o_t), \pi^L(a_t|s_t, o_t), \beta(s_t, o_t))$. The initiation condition I describes an

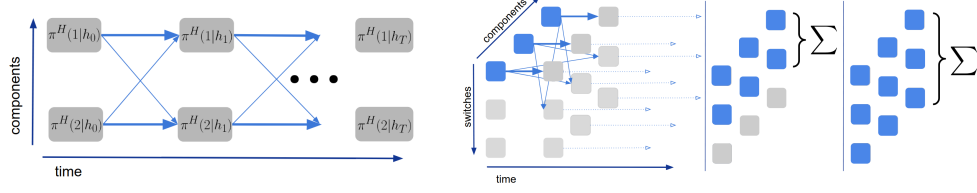


Figure 2: Representation of the dynamic programming forward pass - bold arrows represent connections without switching. Left: example with two options. Right: extension of the graph to explicitly count the number of switches. Marginalization over the dimension of switches determines component probabilities. By limiting over which nodes to sum at every time-step, the optimization can be targeted to lead to fewer switches and more consistent options.

option’s probability to start in a state and is adapted as $I(s_t, o_t) = 1 \forall s_t \in \mathcal{S}$ following [5, 40]. The termination condition $b_t \sim \beta(s_t, o_t)$ denotes a Bernoulli distribution describing the option’s probability to terminate in any given state and the action distribution for a given option is modelled by $\pi^L(a_t|s_t, o_t)$. Every time the agent observes a state, the current option’s termination condition is sampled. If subsequently no option is active, a new option is sampled from the controller $\pi^C(o_t|s_t)$. Finally, we sample from either the continued or new option to generate a new action.

The transitions between options can be described by

$$p(o_t|s_t, o_{t-1}) = \begin{cases} 1 - \beta(s_t, o_{t-1}) + \beta(s_t, o_{t-1})\pi^C(o_t|s_t) & \text{if } o_t = o_{t-1} \\ \beta(s_t, o_{t-1})\pi^C(o_t|s_t) & \text{otherwise} \end{cases} \quad (2)$$

In Equation 3, the joint action-option probability is factorized into the distribution over options conditioned on the trajectory h_t and the option-conditional action distribution, which is only conditioned on the current state s_t . This factorization and the following per time-step exact marginalization over options in Equation 4 enable us to efficiently compute the likelihood of actions and options along off-policy trajectories instead of using option samples and efficiently perform intra-option learning [22] for all options independently of the executed option.

$$\pi_\theta(a_t, o_t|h_t) = \pi^L(a_t|s_t, o_t) \pi^H(o_t|h_t) \quad (3)$$

Following the graphical model in Figure 1, the probability of being in component o_t at time step t across a trajectory h_t can be determined in a recursive manner based on the option probabilities of the previous time-step. For the first time-step, the probabilities are given by the high-level controller $\pi^H(o_0|h_0) = \pi^C(o_0|s_0)$ and for all consecutive steps are computed as follows for M options using the option transition probabilities in Equation 2.

$$\tilde{\pi}^H(o_t|h_t) = \sum_{o_{t-1}=1}^M [p(o_t|s_t, o_{t-1}) \pi^H(o_{t-1}|h_{t-1}) \pi^L(a_{t-1}|s_{t-1}, o_{t-1})] \quad (4)$$

In every step, we normalize the distribution following $\pi^H(o_t|h_t) = \tilde{\pi}^H(o_t|h_t) / \sum_{o'_t=1}^M \tilde{\pi}^H(o'_t|h_t)$. This dynamic programming formulation (similar to [25, 31, 33]) allows the use of automatic differentiation in modern deep learning frameworks (e.g. [1]) to backpropagate through the graph to determine the gradient updates for all policy parameters in the later policy improvement. The method is computationally more efficient than determining updates over all possible sequences of options independently and reduces variance compared to sampling-based approximations with the executed option or new samples during learning. In practice we have found that removing the conditioning of component probabilities on actions (the π_L terms in Equation 4) improves performance and stability. Therefore, we condition only on states and investigate the effects of conditioning on potentially stale actions in off-policy learning in Section 3.4.

Temporal Consistency Using options over longer sequences can help to reduce the search space and simplify exploration [11, 34]. We introduce an additional mechanism to reduce the number of switches between options along a trajectory without introducing an additional weighted loss term. The 2D graph for computing option probabilities along a trajectory in Figure 2 can be extended with a third dimension representing the number of switches between options. Practically, this means that

we are modelling $\pi^H(o_t, n_t|h_t)$ where n_t represents the number of switches until time-step t . We can marginalize over all numbers of switches to determine option probabilities. In order to encourage option consistency across time-steps, we can instead sum over only a subset of nodes for all $n \leq N$ with N smaller than the maximal number of switches leading to $\pi^H(o_t|h_t) = \sum_{n_t=0}^N \pi^H(o_t, n_t|h_t)$.

For the first time-step, only 0 switches are possible and $\pi^H(o_0, n_0|h_0) = 0$ everywhere except for $n_0 = 0$ and $\pi^H(o_0|n_0 = 0, h_0) = \pi^C(o_0|s_0)$. For further time-steps, all edges following option terminations β lead to the next step's option probabilities with increased number of switches $n_{t+1} = n_t + 1$. All edges following option continuation lead to the probabilities for equal number of switches $n_{t+1} = n_t$. This results in the following computation of the joint distribution for $t > 0$:

$$\tilde{\pi}^H(o_t, n_t|h_t) = \sum_{\substack{M, N \\ o_{t-1}=1, \\ n_{t-1}=1}} p(o_t, n_t|s_t, o_{t-1}, n_{t-1}) \pi^H(o_{t-1}, n_{t-1}|h_{t-1}) \pi^L(a_{t-1}|s_{t-1}, o_{t-1}) \quad (5)$$

with the option and switch index transitions $p(o_t, n_t|s_t, o_{t-1}, n_{t-1})$ described in Equation 19 in the Appendix and normalization as $\pi^H(o_t, n_t|h_t) = \tilde{\pi}^H(o_t, n_t|h_t) / \sum_{o'_t=1}^M \sum_{n'_t=1}^L \tilde{\pi}^H(o'_t, n'_t|h_t)$.

We now continue to describe the main policy improvement algorithm, which requires the previously determined option probabilities. The principal three steps are: 1. update the critic following Eq. 6; 2. based on the updated critic, generate an intermediate, non-parametric policy (Eq. 7); 3. update the parametric policy to align to the non-parametric improvement (Eq. 9).

Policy Evaluation For option policies, the critic is a function of s , a , and o since the current option influences the likelihood of future actions and thus rewards. Note that, even though we express the policy as a function of the history h_t , Q is a function of o_t , s_t , a_t , since these are sufficient to render the future trajectory independent of the past (see the graphical model in Figure 1). In the constrained case Q also depends on n_t , which we omit here for clarity. We define the TD(0) objective as

$$\min_{\phi} L(\phi) = \mathbb{E}_{s_t, a_t, o_t \sim \mathcal{D}} \left[(Q_T - Q_{\phi}(s_t, a_t, o_t))^2 \right], \quad (6)$$

where the current states, actions and options are sampled from the current replay buffer \mathcal{D} . For the 1-step target $Q_T = r_t + \gamma \mathbb{E}_{s_{t+1}, a_{t+1}, o_{t+1}} [Q'(s_{t+1}, a_{t+1}, o_{t+1})]$, the next state s_{t+1} is returned from the replay buffer and we estimate the value by sampling actions and options according to $a_{t+1}, o_{t+1} \sim \pi^H(\cdot|h_{t+1})$ following Equation 2.

Policy Improvement We follow an Expectation-Maximization procedure similar to [2, 39], which first computes an improved non-parametric policy and then updates the parametric policy to match this target. Given Q , all we require to optimize option policies is the possibility to sample from the policy and determine the log-likelihood (gradient) of actions and options under the policy given h_t .

The first step of policy improvement provides us with the non-parametric policy $q(a_t, o_t|h_t)$.

$$\max_q J(q) = \mathbb{E}_{a_t, o_t \sim q, s_t \sim \mathcal{D}} [Q_{\phi}(s_t, a_t, o_t)], \text{ s.t. } \mathbb{E}_{h_t \sim \mathcal{D}} [\text{KL}(q(\cdot|h_t) \parallel \pi_{\theta}(\cdot|h_t))] \leq \epsilon_E, \quad (7)$$

where $\text{KL}(\cdot \parallel \cdot)$ denotes the Kullback-Leibler divergence, ϵ_E defines a bound on the KL. We can find the solution to the constrained optimization problem in Eq. (7) in closed-form and obtain

$$q(a_t, o_t|h_t) \propto \pi_{\theta}(a_t, o_t|h_t) \exp(Q_{\phi}(s_t, a_t, o_t)/\eta). \quad (8)$$

Practically speaking, this step computes samples from the previous policy and weights them based on the corresponding temperature-calibrated values of the critic. The temperature parameter η is computed following the dual of the Lagrangian. The derivation and final form of the dual can be found in Appendix C.1, Equation 17.

To align parametric and non-parametric policies in the second step, we minimize their KL divergence.

$$\theta_+ = \arg \min_{\theta} \mathbb{E}_{h_t \sim \mathcal{D}} [\text{KL}(q(\cdot|h_t) \parallel \pi_{\theta}(\cdot|h_t))], \text{ s.t. } \mathbb{E}_{h_t \sim \mathcal{D}} [\mathcal{T}(\pi_{\theta_+}(\cdot|h_t) \parallel \pi_{\theta}(\cdot|h_t))] \leq \epsilon_M \quad (9)$$

The distance function \mathcal{T} in Equation 9 has a trust-region effect and stabilizes learning by constraining the change in the parametric policy. The computed option probabilities from Equation 4 are used in Equation 8 to enable sampling of options as well as Equation 9 to determine and maximize the likelihood of option samples under the policy. We can apply Lagrangian relaxation again and solve the primal as detailed in Appendix C.2. Finally, we describe the complete pseudo-code for HO2 in Algorithm 1, where we use target networks for policy π' and Q-function Q' to stabilize training.

Multi-Task Learning For the multi-task case, we share policies and Q-functions across tasks with details in Appendix A. Additionally, we assign rewards for all tasks to any generated transition data in hindsight to share exploration and data generation functionality across tasks [4, 26, 39].

Algorithm 1 Hindsight Off-policy Options

```

while not done do
  sample trajectories  $\tau$  from replay buffer
  // forward pass along sampled trajectories
  determine component probabilities  $\pi^H(o_t|h_t)$  (Eq. 4)
  sample actions  $a_j$  and options  $o_j$  from  $\pi_\theta(\cdot|h_t)$  (Eq. 3) to estimate expectations
  // compute gradients over batch for policy, Lagrangian multipliers and Q-function
   $\delta_\theta \leftarrow -\nabla_\theta \sum_{h_t \in \tau} \sum_j [\exp(Q_\phi(s_t, a_j, o_j)/\eta) \log \pi_\theta(a_j, o_j|h_t)]$  following Eq. 8 and 9
   $\delta_\eta \leftarrow \nabla_\eta g(\eta) = \nabla_\eta \eta \epsilon + \eta \sum_{h_t \in \tau} \log \sum_j [\exp(Q_\phi(s_t, a_j, o_j)/\eta)]$  following Eq. 17
   $\delta_\phi \leftarrow \nabla_\phi \sum_{(s_t, a_t, o_t) \in \tau} (Q_\phi(s_t, a_t, o_t) - Q_T)^2$  following Eq. 6
  update  $\theta, \eta, \phi$  // apply gradient updates
  if number of iterations = target update then
     $\pi' = \pi_\theta, Q' = Q_\phi$  // update target networks

```

3 Experiments

We begin by investigating the performance of HO2 under a broad set of conditions based on common OpenAI gym [7] domains in the single task case to compare against current work in option learning and off-policy methods (Section 3.1). Additionally, we run pixel-based 3D robotic manipulation experiments for multi-task and transfer learning to investigate scalability and robustness to investigate scalability to considerably more complex domains (Section 3.2). In order to compare the impact of action abstraction in mixture policies and the additional temporal abstraction brought by option policies we compare training mixture-of-Gaussians policies (RHPO [39]) and option policies (HO2) under related training paradigms. In Section 3.3, we additionally perform sequential transfer experiments with pre-trained options to focus on the impact of increased temporal consistency from applying constraints on the number of option switches. Finally, we perform ablations in Section 3.4 to investigate the challenges of robust off-policy learning for options and further improve understanding of various environment and algorithm aspects on task decomposition.

3.1 Single Task Experiments

We compare HO2 (with and without limiting option switches) against competitive baselines for option learning in feature-based continuous action space domains. The baselines include Double Actor-Critic (DAC) [40], Inferred Option Policy Gradient (IOPG) [33] and Option-Critic (OC) [5].

As demonstrated in Figure 3, off-policy learning alone (here: MPO [2]) can improve data-efficiency and can suffice to outperform hierarchical on-policy algorithms such as DAC, IOPG and Option-Critic - emphasizing the importance of a strong underlying policy optimization method and the possibility to build upon recent advances in off-policy learning. We additionally achieve considerable improvements when training mixture policies via RHPO [39] and furthermore accelerate learning

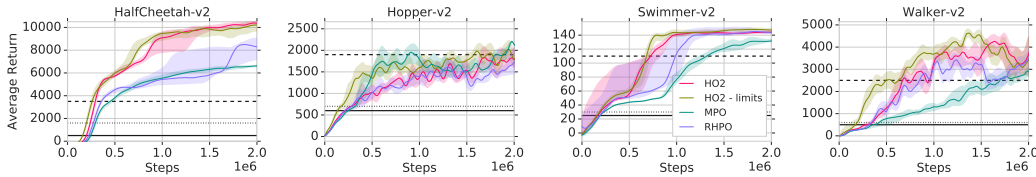


Figure 3: Results on OpenAI gym. Dashed black line represents DAC [40], dotted line represents Option-Critic [5] and solid line represents IOPG [33] (approximate results after 2×10^6 steps from [40]). We limit the maximum number of switches to 5 for HO2-limits. HO2 considerably outperforms existing option learning algorithms.

with temporal abstraction via HO2, which provides the best performance across all tasks. Using the switch constraints for increasing temporal abstraction from Section 2 can provide minor benefits in some tasks but overall has only a minor effect on performance. We further investigate this effect in sequential transfer in Section 3.3.

3.2 Parallel Multi-task Transfer Experiments

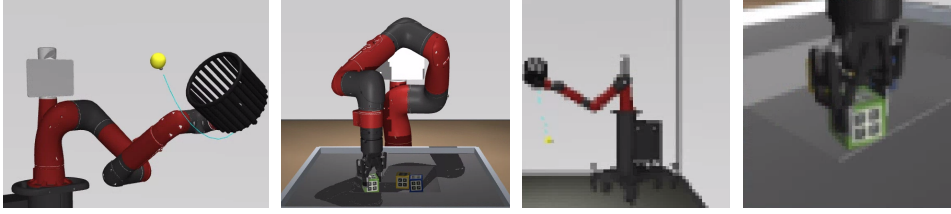


Figure 4: Ball-In-Cup and Stacking. Left: Environments. Right: Example agent observations.

We next focus on investigating HO2 on a set of more complex simulated robotic manipulation tasks - stacking and ball-in-cup (BIC) - as displayed in Figure 4, purely based on robot proprioception and raw pixel inputs (64x64 pixel, 2 cameras for BIC and 3 for stacking). Since the performance of HO2 is relatively independent of switch constraints as seen in Figure 3, we will simplify our figures by focusing on the base method. To improve data efficiency and transfer, we share data between tasks and relabel with task rewards in hindsight [4, 26, 39], which is applied for all algorithms following Section 2, with additional details in Appendix B.

Across all tasks, both RHPO and HO2 outperform a simple Gaussian policy trained via MPO. The difference grows as the task complexity increases and is particularly pronounced for the final stacking tasks in Figure 5. HO2 additionally improves performance over mixture policies (RHPO) demonstrating that the ability to learn temporal abstraction proves beneficial in these domains.

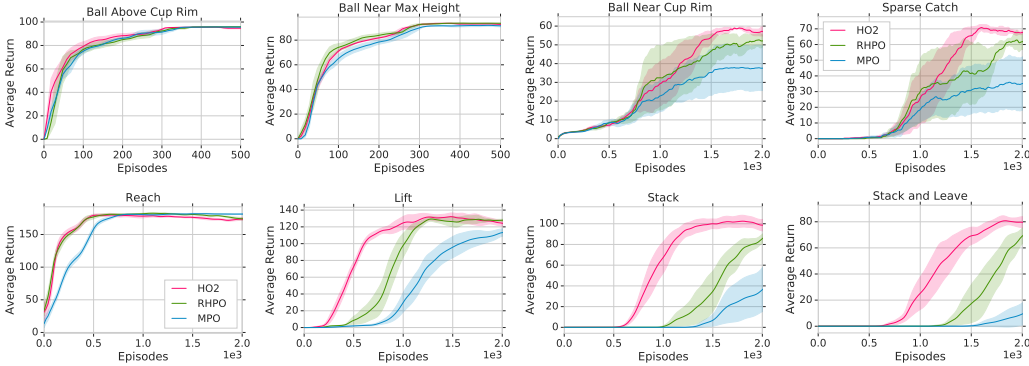


Figure 5: Results for HO2, RHPO and MPO in multi-task domains with pixel-based ball-in-cup (top) and pixel-based block stacking (bottom).

3.3 Sequential Transfer Experiments

There is a difference between enabling the policy to represent temporal abstraction and enforcing or optimizing for it. The introduction of the ability in HO2 helps across all domains. However, there is little benefit in increasing temporal consistency (via limiting the number of switches) in our experiments for training from scratch. In this section, we evaluate this aspect for the sequential transfer case. For these experiments, we first train low-level options for all tasks except for the final, most complex task in each domain. Successively, given this set of pre-trained options, we only train for the final task and compare training with and without limits. We build on the same multi-task domains from Section 3.2: block stacking and BIC based on Sawyer robot arms. Across both domains we can see that more consistent options lead to increased performance in the transfer domain. Intuitively, more consistency and fewer switches lead to a smaller search space for the

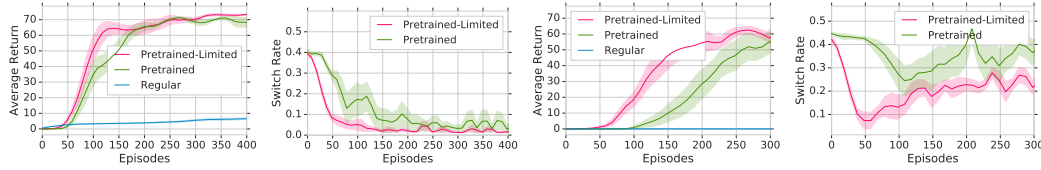


Figure 6: Sequential transfer experiments with limited option switches. Left: BIC. Right: Stack. For both cases, we show the learning curve on final task which demonstrates considerable improvements for limited switches in the sequential transfer case. In addition, we visualize the actual agent option switch rate in the environment during training.

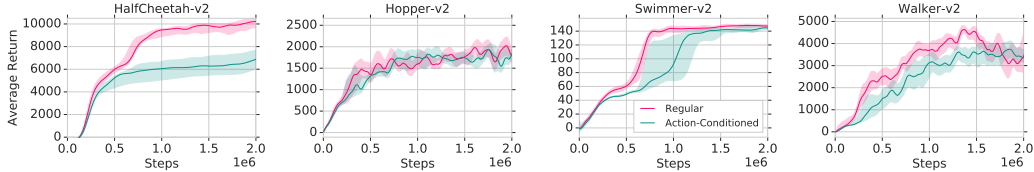


Figure 7: Results on OpenAI gym with/without conditioning of option probabilities on past actions.

high-level controller, by persisting with one behavior for longer after selection. While the same mechanism can also hold for training from scratch, it is likely that the added complexity of extracting beneficial temporal consistency simultaneous to solving the task outweighs the benefits.

3.4 Further Analysis and Ablations

In this section, we investigate different algorithmic aspects to get a better understanding of the approach, and how to achieve robust training of options in an off-policy setting.

Off-policy Option Learning Figure 7 visualizes that across most of our experiments, we find that conditioning component probabilities on the previous timesteps’ action probabilities (see Section 2) detrimental. An explanation for these results can be found in the potential staleness of performed actions with respect to the current policy caused by the off-policy training setup. We additionally include results displaying less impact in the on-policy case in Appendix A.4.

Trust-regions and Robustness Generating trust-region constraints for policy updates has been shown to be beneficial for Gaussian policies [2, 29]. Here we describe the impact of applying different strength constraints on option probabilities (both termination conditions β and the high-level controller π_C). As displayed in Figure 8, the approach is robust across different values, but very weak or strong constraints do negatively affect performance. All additional tasks in the domain can be found in Appendix A.5.

Decomposition and Option Clustering We also apply HO2 to a variety of simple locomotion tasks to investigate how the agent uses its capacity and decomposes behavior into options. In these tasks, the agent body (eg. “Ant”) must go to one of three targets in a room, with the task specified by the target locations and a selected target index. As shown in Figure 9, we find that option decompositions depend on the task and algorithm settings. *Information asymmetry (IA)*, here via providing task information only to the high-level controller, can address degenerate solutions and lead to more specialized options and wider option use. Experiments with a wider variety of bodies and tasks, and further discussion, can be found in Appendix A.1.

4 Related Work

Hierarchy has been investigated in many forms in the context of reinforcement learning to improve data gathering as well as data fitting aspects. Goal-based approaches commonly define a grounded interface between high- and low-level policies such that the high level acts by providing goals to the low level, which is trained to achieve these goals [17, 19, 20, 37]. These methods have been able to overcome very sparse reward domains but commonly require domain knowledge and the crafted interface can limit expressiveness and richness of behaviour.

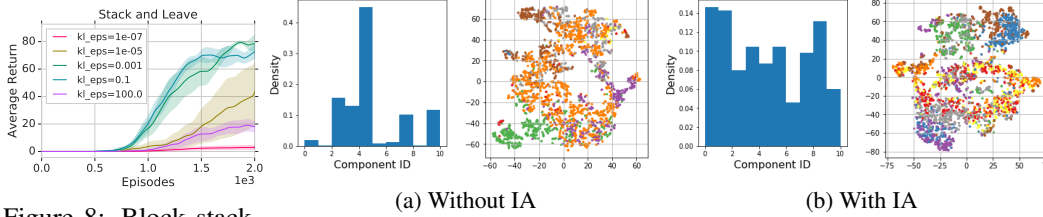


Figure 8: Block stack-
ing results with different
trust-region constraints.

Figure 9: Analysis on Ant locomotion tasks, showing histogram over
options, and t-SNE scatter plots in action space colored by option.

More emergent interfaces within policies have been investigated from an RL-as-inference perspective via policies with continuous latent variables [10, 13, 14, 15, 35, 36]. Related to these approaches, we provide an inference perspective to off-policy option learning and benefit from efficient dynamic programming inference procedures.

Our work is closest related to the option framework [23, 34], which describes policies with an autoregressive, discrete latent space. Option policies commonly use a high-level controller to choose from a set of options or skills which additionally include termination conditions, to enable a skill to represent temporally extended behaviour. Without termination conditions, options can be seen as equivalent to components under a mixture distribution, and this simplified formulation has been applied successfully in different methods [3, 8, 39]. The option framework has been further extended and improved for more practical application [5, 11, 12, 24, 27, 33].

One important step towards increasing the robustness of option learning has been taken in [40] by building on robust (on-policy) policy optimization with PPO [30]. HO2 has similar robustness benefits, but additionally improves data-efficiency by building on off-policy learning, hindsight inference of options, and additional trust-region constraints [2, 39]. Related inference procedures have also been investigated in imitation learning [31] as well as on-policy RL [33]. In addition to inference of suited options in hindsight, off-policy learning enables us to make use of hindsight assignment of rewards for multiple tasks, which has been successfully applied with flat, non-hierarchical policies [4, 26] and goal-based hierarchical approaches [17, 20].

In general, hierarchical approaches have demonstrated significant benefits for compromising between enabling positive transfer and the mitigation of negative interference [6, 28, 39]. Finally, the benefits of options and other modular policy styles have also been applied in the supervised case for learning from demonstration [9, 16, 31].

5 Conclusions

We introduce a novel actor-critic algorithm for robust and efficient training of options and task decomposition in the off-policy setting. The approach outperforms recent work in option learning on common benchmarks, and is able to solve complex, simulated robot manipulation tasks from raw pixel inputs more reliably than competitive baselines. HO2 infers option and action probabilities for trajectories in hindsight, and performs critic-weighted maximum-likelihood estimation by back-propagating through the inference procedure. The ability to infer option choices given a trajectory, allows us to train from off-policy trajectories, including from different tasks, and makes it possible to impose hard constraints on the termination frequency without introducing additional objectives. We investigate the consequences of the off-policy nature of training data, and demonstrate the benefits of trust-region constraints in the hierarchical setting.

We separately analyze the impact of action abstraction (implemented via mixture policies), and temporal abstraction (implemented via the autoregressive modeling of options), and find that both can improve performance. Enforcing temporal consistency of option choice displays limited effect when learning from scratch but is beneficial when transferring pre-trained options to a new task. We investigate the connection between algorithmic aspects (such as information asymmetry) and environment aspects (including the complexity of agent embodiment) with respect to task decomposition and skill clustering. Further work can improve our understanding of how the combination of environment and agent properties affects the decomposition of tasks and use of capacity. Finally, since our method performs (weighted) maximum likelihood learning, it can be naturally adapted to learn structured behavior representations in mixed data regimes, e.g. to learn from combinations of demonstrations, logged data, and online trajectories. This opens up promising directions for future work.

Broader Impact

This work addresses a fundamental topic in reinforcement learning: the ability to learn reusable discrete options or skills. While the underlying technical contributions can be considered a core building block, this work can have a broad impact across a variety of application domains.

The more complex tasks in this paper focus primarily on the robotics domain, and we evaluate our approach on a set of robot tasks. Robotics has the potential for large positive impact, and the ability to interact with objects is fundamental to deploying such systems in the real world. However, care needs to be taken to ensure such methods are not extended to harmful applications, such as military or surveillance use. Further, the increasing deployment of robots in the real world is likely to impact the job market, which is perhaps an issue that needs to be addressed at a government and societal level. These issues will become more significant as these techniques improve and see wider use outside a confined suite of tasks.

Acknowledgments and Disclosure of Funding

The authors would like to thank Tobias Springenberg, Peter Humphreys, and Satinder Singh for helpful discussion and relevant feedback for shaping our submission. We additionally like to acknowledge the support of Francesco Romano, Francesco Nori, and others from the DeepMind robotics lab regarding robotics infrastructure.

References

- [1] Martín Abadi, Paul Barham, Jianmin Chen, Zhifeng Chen, Andy Davis, Jeffrey Dean, Matthieu Devin, Sanjay Ghemawat, Geoffrey Irving, Michael Isard, et al. Tensorflow: A system for large-scale machine learning. In *12th {USENIX} Symposium on Operating Systems Design and Implementation ({OSDI} 16)*, pages 265–283, 2016.
- [2] Abbas Abdolmaleki, Jost Tobias Springenberg, Yuval Tassa, Rémi Munos, Nicolas Heess, and Martin A. Riedmiller. Maximum a posteriori policy optimisation. *CoRR*, abs/1806.06920, 2018.
- [3] Alejandro Agostini and Enric Celaya. Reinforcement learning with a gaussian mixture model. In *The 2010 International Joint Conference on Neural Networks (IJCNN)*, pages 1–8. IEEE, 2010.
- [4] Marcin Andrychowicz, Filip Wolski, Alex Ray, Jonas Schneider, Rachel Fong, Peter Welinder, Bob McGrew, Josh Tobin, Pieter Abbeel, and Wojciech Zaremba. Hindsight experience replay. In *Advances in Neural Information Processing Systems*, pages 5048–5058, 2017.
- [5] Pierre-Luc Bacon, Jean Harb, and Doina Precup. The option-critic architecture. In *Thirty-First AAAI Conference on Artificial Intelligence*, 2017.
- [6] Christopher M Bishop. Mixture density networks. Technical report, Citeseer, 1994.
- [7] Greg Brockman, Vicki Cheung, Ludwig Pettersson, Jonas Schneider, John Schulman, Jie Tang, and Wojciech Zaremba. Openai gym. *ArXiv*, abs/1606.01540, 2016.
- [8] Christian Daniel, Gerhard Neumann, Oliver Kroemer, and Jan Peters. Hierarchical relative entropy policy search. *The Journal of Machine Learning Research*, 17(1):3190–3239, 2016.
- [9] Roy Fox, Sanjay Krishnan, Ion Stoica, and Ken Goldberg. Multi-level discovery of deep options. *arXiv preprint arXiv:1703.08294*, 2017.
- [10] Tuomas Haarnoja, Kristian Hartikainen, Pieter Abbeel, and Sergey Levine. Latent space policies for hierarchical reinforcement learning. In *International Conference on Machine Learning*, pages 1846–1855, 2018.
- [11] Jean Harb, Pierre-Luc Bacon, Martin Klissarov, and Doina Precup. When waiting is not an option: Learning options with a deliberation cost. In *Thirty-Second AAAI Conference on Artificial Intelligence*, 2018.

- [12] Anna Harutyunyan, Will Dabney, Diana Borsa, Nicolas Heess, Rémi Munos, and Doina Precup. The termination critic. *CoRR*, abs/1902.09996, 2019.
- [13] Karol Hausman, Jost Tobias Springenberg, Ziyu Wang, Nicolas Heess, and Martin Riedmiller. Learning an embedding space for transferable robot skills. In *International Conference on Learning Representations*, 2018.
- [14] Nicolas Heess, Greg Wayne, Yuval Tassa, Timothy Lillicrap, Martin Riedmiller, and David Silver. Learning and transfer of modulated locomotor controllers. *arXiv preprint arXiv:1610.05182*, 2016.
- [15] Maximilian Igl, Andrew Gambardella, Nantas Nardelli, N Siddharth, Wendelin Böhmer, and Shimon Whiteson. Multitask soft option learning. *arXiv preprint arXiv:1904.01033*, 2019.
- [16] Sanjay Krishnan, Roy Fox, Ion Stoica, and Ken Goldberg. Ddco: Discovery of deep continuous options for robot learning from demonstrations. *arXiv preprint arXiv:1710.05421*, 2017.
- [17] Andrew Levy, George Konidaris, Robert Platt, and Kate Saenko. Learning multi-level hierarchies with hindsight. *arXiv preprint arXiv:1712.00948*, 2017.
- [18] Alexander C Li, Carlos Florensa, Ignasi Clavera, and Pieter Abbeel. Sub-policy adaptation for hierarchical reinforcement learning. *arXiv preprint arXiv:1906.05862*, 2019.
- [19] Ofir Nachum, Shixiang Gu, Honglak Lee, and Sergey Levine. Near-optimal representation learning for hierarchical reinforcement learning. *arXiv preprint arXiv:1810.01257*, 2018.
- [20] Ofir Nachum, Shixiang Shane Gu, Honglak Lee, and Sergey Levine. Data-efficient hierarchical reinforcement learning. In *Advances in Neural Information Processing Systems*, pages 3303–3313, 2018.
- [21] OpenAI, Marcin Andrychowicz, Bowen Baker, Maciek Chociej, Rafal Józefowicz, Bob McGrew, Jakub W. Pachocki, Jakub Pachocki, Arthur Petron, Matthias Plappert, Glenn Powell, Alex Ray, Jonas Schneider, Szymon Sidor, Josh Tobin, Peter Welinder, Lilian Weng, and Wojciech Zaremba. Learning dexterous in-hand manipulation. *CoRR*, abs/1808.00177, 2018.
- [22] Doina Precup. *Temporal abstraction in reinforcement learning*. University of Massachusetts Amherst, 2000.
- [23] Doina Precup. Temporal abstraction in reinforcement learning. 2001.
- [24] Doina Precup, Cosmin Paduraru, Anna Koop, Richard S Sutton, and Satinder P. Singh. Off-policy learning with options and recognizers. In Y. Weiss, B. Schölkopf, and J. C. Platt, editors, *Advances in Neural Information Processing Systems 18*, pages 1097–1104. MIT Press, 2006.
- [25] Lawrence R Rabiner. A tutorial on hidden markov models and selected applications in speech recognition. *Proceedings of the IEEE*, 77(2):257–286, 1989.
- [26] Martin Riedmiller, Roland Hafner, Thomas Lampe, Michael Neunert, Jonas Degraeve, Tom Van de Wiele, Volodymyr Mnih, Nicolas Heess, and Jost Tobias Springenberg. Learning by playing-solving sparse reward tasks from scratch. *arXiv preprint arXiv:1802.10567*, 2018.
- [27] Matthew Riemer, Miao Liu, and Gerald Tesauro. Learning abstract options. In *Advances in Neural Information Processing Systems*, pages 10424–10434, 2018.
- [28] Michael T Rosenstein, Zvika Marx, Leslie Pack Kaelbling, and Thomas G Dietterich. To transfer or not to transfer. In *NIPS 2005 workshop on transfer learning*, volume 898, pages 1–4, 2005.
- [29] John Schulman, Sergey Levine, Philipp Moritz, Michael Jordan, and Pieter Abbeel. Trust region policy optimization. In *Proceedings of the 32nd International Conference on International Conference on Machine Learning-Volume 37*, pages 1889–1897. JMLR. org, 2015.
- [30] John Schulman, Filip Wolski, Prafulla Dhariwal, Alec Radford, and Oleg Klimov. Proximal policy optimization algorithms. *arXiv preprint arXiv:1707.06347*, 2017.

- [31] Kyriacos Shiarlis, Markus Wulfmeier, Sasha Salter, Shimon Whiteson, and Ingmar Posner. Taco: Learning task decomposition via temporal alignment for control. In *International Conference on Machine Learning*, pages 4661–4670, 2018.
- [32] David Silver, Julian Schrittwieser, Karen Simonyan, Ioannis Antonoglou, Aja Huang, Arthur Guez, Thomas Hubert, Lucas Baker, Matthew Lai, Adrian Bolton, et al. Mastering the game of go without human knowledge. *Nature*, 550(7676):354, 2017.
- [33] Matthew Smith, Herke Hoof, and Joelle Pineau. An inference-based policy gradient method for learning options. In *International Conference on Machine Learning*, pages 4703–4712, 2018.
- [34] Richard Sutton, Doina Precup, and Satinder Singh. Between mdps and semi-mdps: A framework for temporal abstraction in reinforcement learning. *Artificial intelligence*, 112(1-2):181–211, 1999.
- [35] Yee Whye Teh, Victor Bapst, Wojciech Marian Czarnecki, John Quan, James Kirkpatrick, Raia Hadsell, Nicolas Heess, and Razvan Pascanu. Distral: Robust multitask reinforcement learning. *CoRR*, abs/1707.04175, 2017.
- [36] Dhruva Tirumala, Hyeonwoo Noh, Alexandre Galashov, Leonard Hasenclever, Arun Ahuja, Greg Wayne, Razvan Pascanu, Yee Whye Teh, and Nicolas Heess. Exploiting hierarchy for learning and transfer in kl-regularized rl. *arXiv preprint arXiv:1903.07438*, 2019.
- [37] Alexander Sasha Vezhnevets, Simon Osindero, Tom Schaul, Nicolas Heess, Max Jaderberg, David Silver, and Koray Kavukcuoglu. Feudal networks for hierarchical reinforcement learning. In *Proceedings of the 34th International Conference on Machine Learning-Volume 70*, pages 3540–3549. JMLR. org, 2017.
- [38] Oriol Vinyals, Igor Babuschkin, Wojciech M Czarnecki, Michaël Mathieu, Andrew Dudzik, Junyoung Chung, David H Choi, Richard Powell, Timo Ewalds, Petko Georgiev, et al. Grandmaster level in starcraft ii using multi-agent reinforcement learning. *Nature*, 575(7782):350–354, 2019.
- [39] Markus Wulfmeier, Abbas Abdolmaleki, Roland Hafner, Jost Tobias Springenberg, Michael Neunert, Tim Hertweck, Thomas Lampe, Noah Siegel, Nicolas Heess, and Martin Riedmiller. Regularized hierarchical policies for compositional transfer in robotics. *arXiv preprint arXiv:1906.11228*, 2019.
- [40] Shangdong Zhang and Shimon Whiteson. Dac: The double actor-critic architecture for learning options. In *Advances in Neural Information Processing Systems*, pages 2010–2020, 2019.

A Additional Experiments

A.1 Decomposition and Option Clustering

We further deploy HO2 on a set of simple locomotion tasks, where the goal is for an agent to move to one of three randomized target locations in a square room. These are specified as a set of target locations and a task index to select the target of interest.

The main research questions we aim to answer (both qualitatively and quantitatively) are: (1) How do the discovered options specialize and represent different behaviors?; and (2) How is this decomposition affected by variations in the task, embodiment, or algorithmic properties of the agent? To answer these questions, we investigate a number of variations:

- Three bodies: a quadruped with two (“Ant”) or three (“Quad”) torque-controlled joints on each leg, and a rolling ball (“Ball”) controlled by applying yaw and forward roll torques.
- With or without *information asymmetry* (IA) between high- and low-level controllers, where the task index and target positions are withheld from the options and only provided to the categorical option controller.
- With or without limited number of switches in the optimization.

Information-asymmetry (IA) in particular, has recently been shown to be effective for learning general skills: by withholding task-information from low-level options, they can learn task-agnostic, temporally-consistent behaviors that can be composed by the option controller to solve a task. This mirrors the setup in the aforementioned Sawyer tasks, where the task information is only fed to the high-level controller.

For each of the different cases, we qualitatively evaluate the trained agent over 100 episodes, and generate histograms over the different options used, and scatter plots to indicate how options cluster the state/action spaces and task information. We also present quantitative measures (over 5 seeds) to accompany these plots, in the form of (1) Silhouette score, a measure of clustering accuracy based on inter- and intra-cluster distances¹; and (2) entropy over the option histogram, to quantify diversity. The quantitative results are shown in Table 1, and the qualitative plots are shown in Figure 10. Details and images of the environment are in Section B.4.

	Scenario	Option entropy	Switch rate	Cluster score (actions)	Cluster score (states)	Cluster score (tasks)
Regular	Ball	No IA	2.105 ± 0.074	0.196 ± 0.010	-0.269 ± 0.058	-0.110 ± 0.025
		With IA	2.123 ± 0.066	0.346 ± 0.024	-0.056 ± 0.024	-0.164 ± 0.051
	Ant	No IA	1.583 ± 0.277	0.268 ± 0.043	-0.148 ± 0.034	-0.182 ± 0.068
		With IA	2.119 ± 0.073	0.303 ± 0.019	-0.053 ± 0.021	-0.066 ± 0.024
	Quad	No IA	1.792 ± 0.127	0.336 ± 0.019	-0.078 ± 0.064	-0.113 ± 0.035
		With IA	2.210 ± 0.037	0.403 ± 0.014	0.029 ± 0.029	-0.040 ± 0.003
Limited Switches	Ball	No IA	1.804 ± 0.214	0.020 ± 0.009	-0.304 ± 0.040	-0.250 ± 0.135
		With IA	2.233 ± 0.027	0.142 ± 0.015	-0.132 ± 0.035	-0.113 ± 0.043
	Ant	No IA	1.600 ± 0.076	0.073 ± 0.014	-0.124 ± 0.017	-0.155 ± 0.067
		With IA	2.222 ± 0.043	0.141 ± 0.015	-0.052 ± 0.011	-0.054 ± 0.014
	Quad	No IA	1.549 ± 0.293	0.185 ± 0.029	-0.075 ± 0.036	-0.126 ± 0.030
		With IA	2.231 ± 0.042	0.167 ± 0.025	-0.029 ± 0.029	-0.032 ± 0.004

Table 1: Quantitative results indicating the diversity of options used (entropy), and clustering accuracy in action and state spaces (silhouette score), with and without information asymmetry (IA), and with or without limited number of switches. Higher values indicate greater separability by option / component.

The results show a number of trends. Firstly, the usage of IA leads to a greater diversity of options used, across all bodies. Secondly, with IA, the options tend to lead to specialized actions, as demonstrated by the clearer option separation in action space. In the case of the 2D action space of the ball, the options correspond to turning left or right (y-axis) at different forward torques (x-axis). Thirdly, while the simple Ball can learn these high-level body-agnostic behaviors, the options for

¹The silhouette score is a value in $[-1, 1]$ with higher values indicating cluster separability. We note that the values obtained in this setting do not correspond to high *absolute* separability, as multiple options can be used to model the same skill or behavior abstraction. We are instead interested in the *relative* clustering score for different scenarios.

more complex bodies have greater switch rates that suggest the learned behaviors may be related to lower-level motor behaviors over a shorter timescale. Lastly, limiting the number of switches during marginalization does indeed lead to a lower switch rate between options, without hampering the ability of the agent to complete the task.

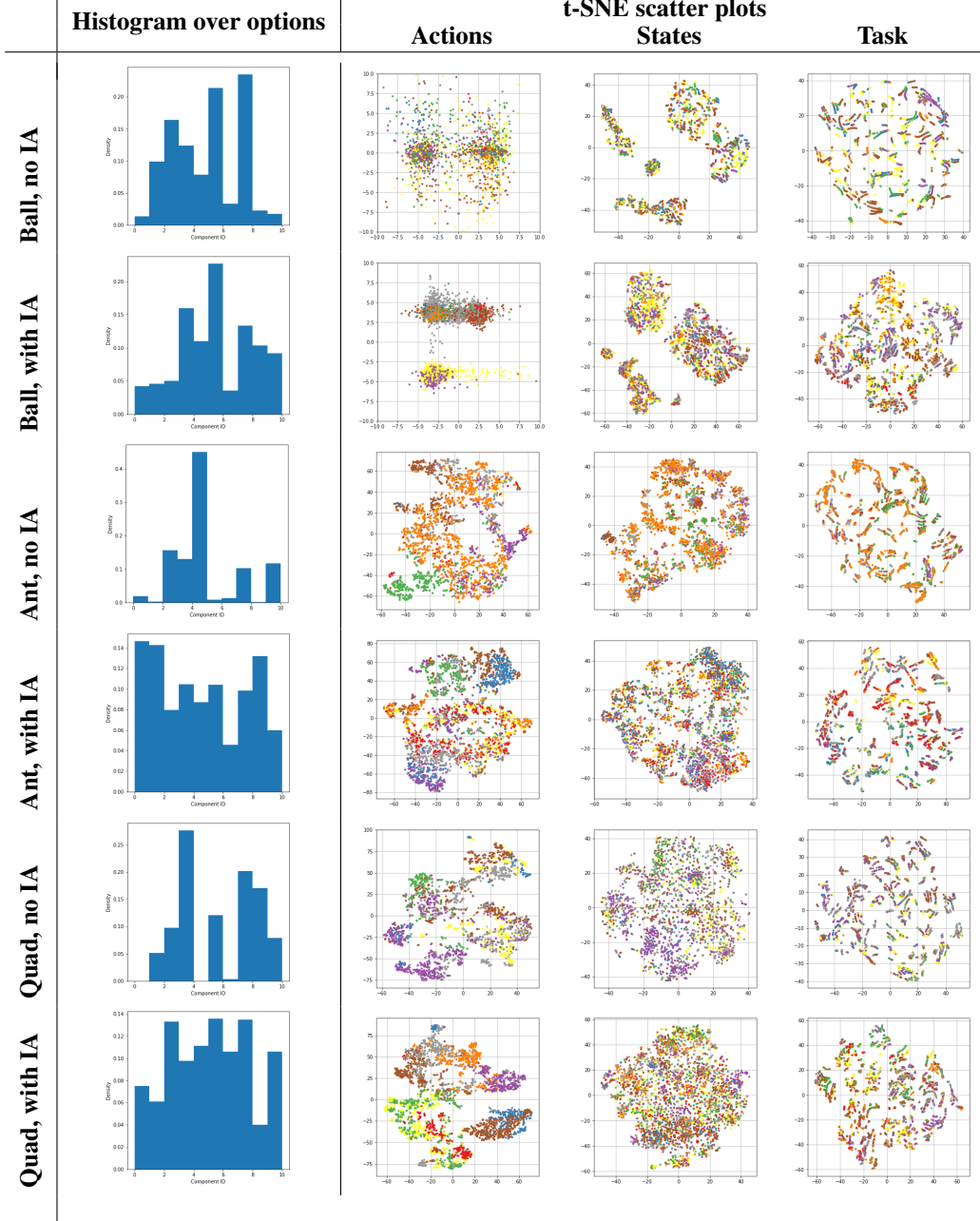


Figure 10: Qualitative results for the three bodies (Ball, Ant, Quad) without limited switches, both with and without IA, obtained over 100 evaluation episodes. **Left:** the histogram over different options used by each agent; **Centre to right:** scatter plots of the action space, state space, and task information, colored by the corresponding option selected. Each of these spaces has been projected to 2D using t-SNE, except for the two-dimensional action space for Ball, which is plotted directly. For each case, care has been taken to choose a median / representative model out of 5 seeds.

A.2 Multi-Task Experiments

The complete results for all pixel and proprioception based multitask experiments for ball-in-cup and stacking can be respectively found in Figures 11 and 12. Both RHPO and HO2 outperform a simple Gaussian policy trained via MPO. HO2 additionally improves performance over mixture policies (RHPO) demonstrating that the ability to learn temporal abstraction proves beneficial in these domains. The difference grows as the task complexity increases and is particularly pronounced for the final stacking tasks.

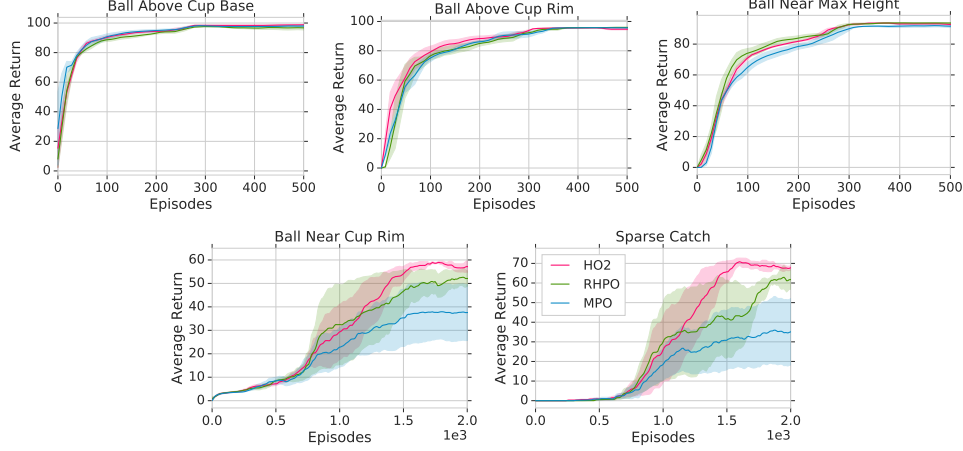


Figure 11: Complete results on pixel-based ball-in-cup experiments.

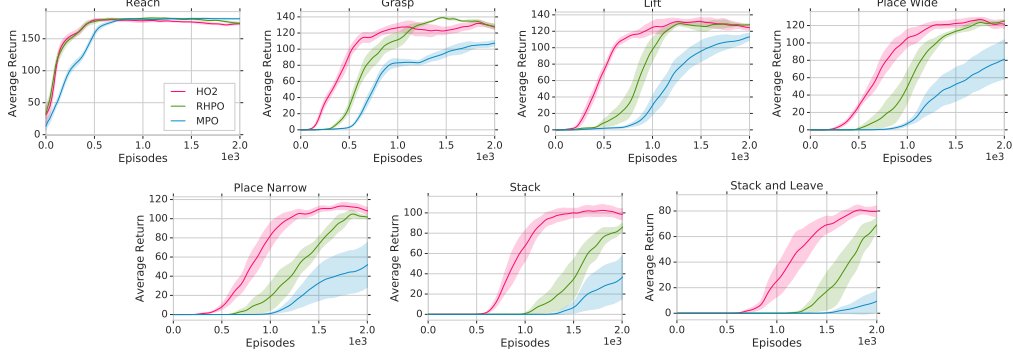


Figure 12: Complete results on pixel-based stacking experiments.

A.3 Task-agnostic Terminations

The complete results for all experiments with task-agnostic terminations can be found in Figure 13.

The perspective of options as task-independent skills with termination conditions as being part of a skill, leads to termination conditions which are also task independent. We show that at least in this limited set of experiments, the perspective of task-dependent termination conditions - i.e. with access to task information - which can be understood as part of the high-level control mechanism for activating options improves performance. Intuitively, by removing task information from the termination conditions, we constrain the space of solutions which first accelerates training slightly but limits final performance. It additionally shows that while we benefit when sharing options across tasks, each task gains from controlling the length of these options independently. Based on these results, the termination conditions across all other multi-task experiments are conditioned on the active task.

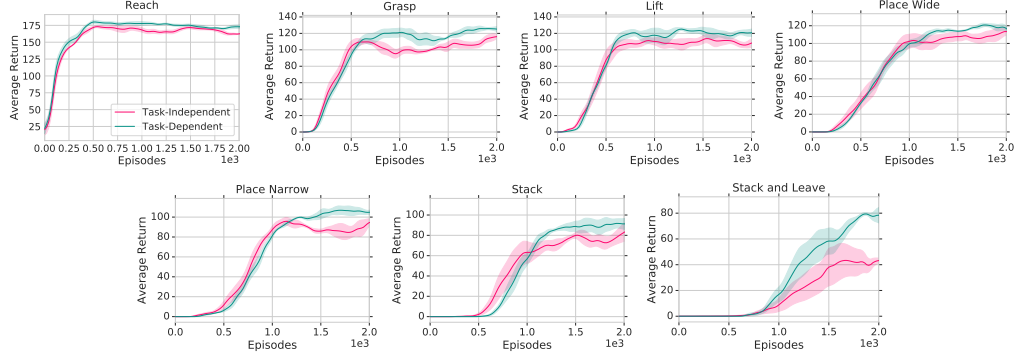


Figure 13: Complete results on multi-task block stacking with and without conditioning termination conditions on tasks.

A.4 Off-Policy Option Learning

The complete results for all experiments with and without action-conditional inference procedure can be found in Figure 14.

In order to train in a more on-policy regime, we reduce the size of the replay buffer by two orders of magnitude and increase the ratio between data generation (actor steps) and data fitting (learner steps) by one order of magnitude. The resulting algorithm is run without any additional hyperparameter tuning to provide an insight into the effect of conditioning on action probabilities under options in the inference procedure. We can see that in the on-policy case the impact of this change is less pronounced. Across all cases, we were unable to generate significant performance gains by including action conditioning into the inference procedure.

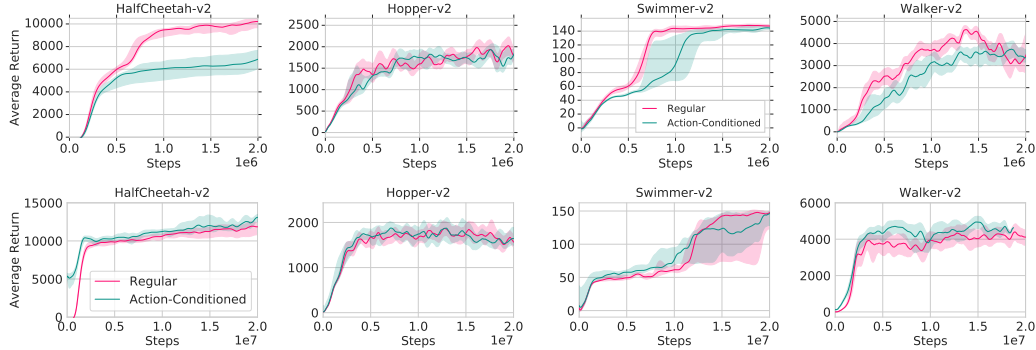


Figure 14: Complete results on OpenAI gym with and without conditioning component probabilities on past executed actions. For the off-policy (top) and on-policy case (bottom). The on-policy approaches uses data considerably less efficiently and the x-axis is correspondingly adapted.

A.5 Trust-region Constraints

The complete results for all trust-region ablation experiments can be found in Figure 15.

With the exception of very high or very low constraints, the approach trains robustly, but performance drops considerably when we remove the constraint fully.

A.6 Exact Inference vs Sampling-based Approximation

To investigate the impact of probabilistic inference of posterior option distributions $\pi_H(o_t|h_t)$ along any given trajectory instead of using sampling-based approximations, we perform additional ablations displayed in Figure 16. We compare HO2 with an ablation of HO2 where we do not compute the option probabilities along a trajectory following Equation 4 but instead use an approximation

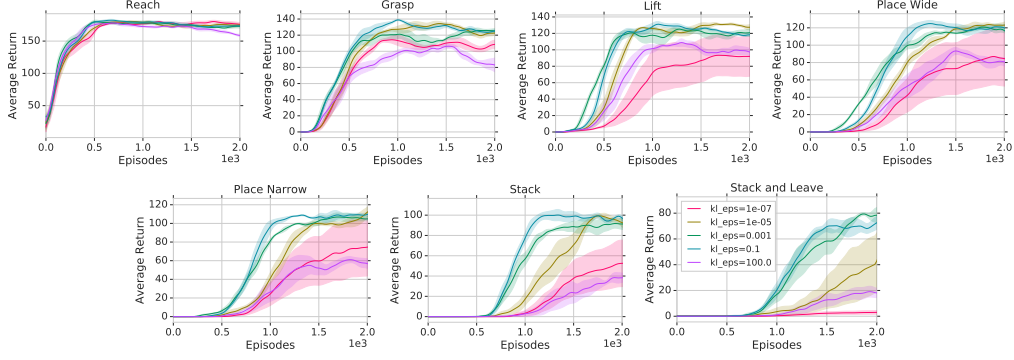


Figure 15: Complete results on block stacking with varying trust-region constraints for both termination conditions β and the high-level controller π_C .

with only concrete option samples propagating across time-steps. For generating action samples, we therefore sample options for every time-step along a trajectory without keeping a complete distribution over options and sample actions only from the active option at every time-step. For determining the likelihood of actions and options for every time-step, we rely on Equation 2 based the sampled options of the previous time-step. By using samples and the critic-weighted update procedure from Equation 9, we can only generate gradients for the policy for the current time-step instead of backpropagating through the whole inference procedure. We find that using both samples from executed options reloaded from the buffer as well as new samples during learning both reduces performance. However, in the Hopper-v2 environment, sampling during learning performs slightly better than inferring options.

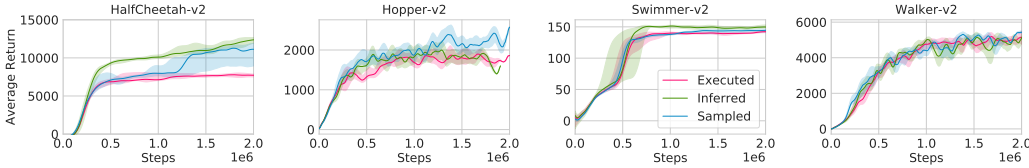


Figure 16: Ablation results comparing inferred options with sampled options during learning (sampled) and during execution (executed). The ablation is run with five actors instead of a single one as used in the single task experiments in order to generate results faster.

B Additional Experiment Details

B.1 Single Task Experiments

All experiments are run with asynchronous learner and actors. For the single task experiments, we use a single actor and report performance over the number of transitions generated. Following [39], both HO2 and RHPO use different biases for the initial mean of all options or mixture components - distributed between minimum and maximum action output. This provides a small but non-negligible benefit and supports specialization of individual options. In line with our baselines (DAC [40], IOPG [33], Option Critic [5]) we use 4 options or mixture components for the OpenAI gym experiments. We run all experiments with 5 samples and report variance and mean. All single task experiments are run with a single actor in a distributed setting.

B.2 Multi-Task Experiments

Shared across all algorithms, we use 3-layer convolutional policy and Q-function torsos with [128, 64, 64] feature channels, [(4, 4), (3, 3), (3, 3)] as kernels and stride 2. For all multitask domains, we build on information asymmetry and only provide task information as input to the high-level controller and termination conditions to create additional incentive for the options to specialize. The Q-function has access to all observations (see the corresponding tables in this section). We follow [26, 39] and

Hyperparameters	HO2	RHPO	MPO
Policy net		256-256	
Number of actions sampled per state		20	
Q function net		256-256	
Number of components		4	NA
ϵ		0.1	
ϵ_μ		5e-4	
ϵ_Σ		5e-5	
ϵ_α		1e-4	NA
ϵ_t	1e-4		NA
Discount factor (γ)		0.99	
Adam learning rate		3d-4	
Replay buffer size		2e6	
Target network update period		200	
Batch size		256	
Activation function		elu	
Layer norm on first layer		Yes	
Tanh on output of layer norm		Yes	
Tanh on input actions to Q-function		Yes	
Retrace sequence length		8	

Table 2: Hyperparameters - Single Task

assign rewards for all possible tasks to trajectories when adding data to the replay buffer independent of the generating policy.

Hyperparameters	HO2	RHPO	MPO
Policy torso			
(shared across tasks)	256		512
Policy task-dependent heads	100 (categorical)		200
Policy shared heads	100 (components)		NA
Policy task-dependent terminations	100 (terminations)	NA	NA
ϵ_μ		1e-3	
ϵ_Σ		1e-5	
ϵ_α		1e-4	NA
ϵ_t	1e-4		NA
Number of action samples		20	
Q function torso			
(shared across tasks)		400	
Q function head (per task)		300	
Number of components	number of tasks		NA
Replay buffer size		1e6	
Target network update period		500	
Batch size		256	

Table 3: Hyperparameters. Values are taken from the single task experiments with the above mentioned changes.

Stacking The setup consists of a Sawyer robot arm mounted on a table and equipped with a Robotiq 2F-85 parallel gripper. In front of the robot there is a basket of size 20x20 cm which contains three cubes with an edge length of 5 cm (see Figure 4).

The agent is provided with proprioception information for the arm (joint positions, velocities and torques), and the tool center point position computed via forward kinematics. For the gripper, it

receives the motor position and velocity, as well as a binary grasp flag. It also receives a wrist sensor's force and torque readings. Finally, it is provided with three RGB camera images at 64×64 resolution. At each time step, a history of two previous observations (except for the images) is provided to the agent, along with the last two joint control commands. The observation space is detailed in Table 5. All stacking experiments are run with 50 actors in parallel and reported over the current episodes generated by any actor.

The robot arm is controlled in Cartesian velocity mode at 20Hz. The action space for the agent is 5-dimensional, as detailed in Table 4. The gripper movement is also restricted to a cubic volume above the basket using virtual walls.

Table 4: Action space for the Sawyer Stacking experiments.

Entry	Dims	Unit	Range
Translational Velocity in x, y, z	3	m/s	[-0.07, 0.07]
Wrist Rotation Velocity	1	rad/s	[-1, 1]
Finger speed	1	tics/s	[-255, 255]

Table 5: Observations for the Sawyer Stacking experiments. The TCP's pose is represented as its world coordinate position and quaternion. In the table, m denotes meters, rad denotes radians, and q refers to a quaternion in arbitrary units (au).

Entry	Dims	Unit	History
Joint Position (Arm)	7	rad	2
Joint Velocity (Arm)	7	rad/s	2
Joint Torque (Arm)	7	Nm	2
Joint Position (Hand)	1	tics	2
Joint Velocity (Hand)	1	tics/s	2
Force-Torque (Wrist)	6	N, Nm	2
Binary Grasp Sensor	1	au	2
TCP Pose	7	m, au	2
Camera images	$3 \times 64 \times 64 \times 3$	R/G/B value	0
Last Control Command	8	rad/s, tics/s	2

$$stol(v, \epsilon, r) = \begin{cases} 1 & \text{iff } |v| < \epsilon \\ 1 - \tanh^2\left(\frac{\text{atanh}(\sqrt{0.95})}{r}|v|\right) & \text{else} \end{cases} \quad (10)$$

$$slin(v, \epsilon_{min}, \epsilon_{max}) = \begin{cases} 0 & \text{iff } v < \epsilon_{min} \\ 1 & \text{iff } v > \epsilon_{max} \\ \frac{v - \epsilon_{min}}{\epsilon_{max} - \epsilon_{min}} & \text{else} \end{cases} \quad (11)$$

$$btol(v, \epsilon) = \begin{cases} 1 & \text{iff } |v| < \epsilon \\ 0 & \text{else} \end{cases} \quad (12)$$

- *REACH*(G): $stol(d(TCP, G), 0.02, 0.15)$:
Minimize the distance of the TCP to the green cube.
- *GRASP*:
Activate grasp sensor of gripper ("inward grasp signal" of Robotiq gripper)
- *LIFT*(G): $slin(G, 0.03, 0.10)$
Increase z coordinate of an object more than 3cm relative to the table.
- *PLACE_WIDE*(G, Y): $stol(d(G, Y + [0, 0, 0.05]), 0.01, 0.20)$
Bring green cube to a position 5cm above the yellow cube.
- *PLACE_NARROW*(G, Y): $stol(d(G, Y + [0, 0, 0.05]), 0.00, 0.01)$:
Like *PLACE_WIDE*(G, Y) but more precise.

- $STACK(G, Y)$: $btol(d_{xy}(G, Y), 0.03) * btol(d_z(G, Y) + 0.05, 0.01) * (1 - GRASP)$
Sparse binary reward for bringing the green cube on top of the yellow one (with 3cm tolerance horizontally and 1cm vertically) and disengaging the grasp sensor.
- $STACK_AND_LEAVE(G, Y)$: $stol(d_z(TCP, G) + 0.10, 0.03, 0.10) * STACK(G, Y)$
Like $STACK(G, Y)$, but needs to move the arm 10cm above the green cube.

Ball-In-Cup This task consists of a Sawyer robot arm mounted on a pedestal. A partially see-through cup structure with a radius of 11cm and height of 17cm is attached to the wrist flange. Between cup and wrist there is a ball bearing, to which a yellow ball of 4.9cm diameter is attached via a string of 46.5cm length (see Figure 4).

Most of the settings for the experiment align with the stacking task. The agent is provided with proprioception information for the arm (joint positions, velocities and torques), and the tool center point and cup positions computed via forward kinematics. It is also provided with two RGB camera images at 64×64 resolution. At each time step, a history of two previous observations (except for the images) is provided to the agent, along with the last two joint control commands. The observation space is detailed in Table 7. All BIC experiments are run with 20 actors in parallel and reported over the current episodes generated by any actor.

The position of the ball in the cup’s coordinate frame is available for reward computation, but not exposed to the agent. The robot arm is controlled in joint velocity mode at 20Hz. The action space for the agent is 4-dimensional, with only 4 out of 7 joints being actuated, in order to avoid self-collision. Details are provided in Table 4.

Table 6: Action space for the Sawyer Ball-in-Cup experiments.

Entry	Dims	Unit	Range
Rotational Joint Velocity for joints 1, 2, 6 and 7	4	rad/s	[-2, 2]

Table 7: Observations for the Sawyer Ball-in-Cup experiments. In the table, m denotes meters, rad denotes radians, and q refers to a quaternion in arbitrary units (au). Note: the joint velocity and command represent the robot’s internal state; the 3 degrees of freedom that were fixed provide a constant input of 0.

Entry	Dims	Unit
Joint Position (Arm)	7	rad
Joint Velocity (Arm)	7	rad/s
TCP Pose	7	m, au
Camera images	$2 \times 64 \times 64 \times 3$	R/G/B value
Last Control Command	7	rad/s

Let B_A be the Cartesian position in meters of the ball in the cup’s coordinate frame (with an origin at the center of the cup’s bottom), along axes $A \in \{x, y, z\}$.

- **CATCH**: $0.17 > B_z > 0$ and $\|B_{xy}\|_2 < 0.11$
Binary reward if the ball is inside the volume of the cup.
- **BALL_ABOVE_BASE**: $B_z > 0$
Binary reward if the ball is above the bottom plane of the cup.
- **BALL_ABOVE_RIM**: $B_z > 0.17$
Binary reward if the ball is above the top plane of the cup.
- **BALL_NEAR_MAX**: $B_z > 0.3$
Binary reward if the ball is near the maximum possible height above the cup.
- **BALL_NEAR_RIM**: $1 - \tanh^2\left(\frac{\operatorname{atanh}(\sqrt{0.95})}{0.5}\right) \times \|B_{xyz} - (0, 0, 0.17)\|_2$
Shaped distance of the ball to the center of the cup opening (0.95 loss at a distance of 0.5).

B.3 Sequential Transfer Experiments

The sequential transfer experiments are performed with the same settings as their multitask equivalents. However, they rely on a pre-training step in which we take all but the final task in each domain and train HO2 to pre-train options which we then transfer with new high-level controller on the final task. Fine-tuning of the options is enabled as we find that it produces slightly better performance. Only data used for the final training step is reported but all both approaches were trained for the same amount of data during pretraining until convergence.

B.4 Locomotion experiments

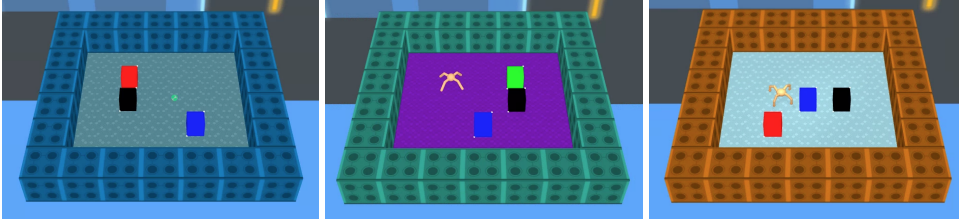


Figure 17: The environment used for simple locomotion tasks with Ball (left), Ant (center) and Quadruped (right).

Figure 17 shows examples of the environment for the different bodies used. In addition to proprioceptive agent state information (which includes the body height, position of the end-effectors, the positions and velocities of its joints and sensor readings from an accelerometer, gyroscope and velocimeter attached to its torso), the state space also includes the ego-centric coordinates of all target locations and a categorical index specifying the task of interest. Table 8 contains an overview of the observations and action dimensions for this task. The agent receives a sparse reward of +60 if part of its body reaches a square surrounding the predicate location, and 0 otherwise. Both the agent spawn location and target locations are randomized at the start of each episode, ensuring that the agent must use both the task index and target locations to solve the task.

Table 8: Observations for the *go to one of 3 targets* task with 'Ball' and 'Ant'.

Entry	Dimensionality
Task Index	3
Target locations	9
Proprioception (Ball)	16
Proprioception (Ant)	41
Proprioception (Quad)	57
Action Dim (Ball)	2
Action Dim (Ant)	8
Action Dim (Quad)	12

C Additional Derivations

In this section we explain the derivations for training option policies with options parameterized as Gaussian distributions. Each policy improvement step is split into two parts: non-parametric and parametric update.

C.1 Non-parametric Option Policy Update

In order to obtain the non-parametric policy improvement we optimize the following equation:

$$\begin{aligned}
& \max_q \mathbb{E}_{h_t \sim p(h_t)} [\mathbb{E}_{a_t, o_t \sim q} [Q_\phi(s_t, a_t, o_t)]] \\
& s.t. \mathbb{E}_{h_t \sim p(h_t)} [\text{KL}(q(\cdot|h_t), \pi_\theta(\cdot|h_t))] < \epsilon_E \\
& s.t. \mathbb{E}_{h_t \sim p(h_t)} [\mathbb{E}_{q(a_t, o_t|h_t)} [1]] = 1.
\end{aligned}$$

for each step t of a trajectory, where $h_t = \{s_t, a_{t-1}, s_{t-1}, \dots, a_0, s_0\}$ represents the history of states and actions and $p(h_t)$ describes the distribution over histories for time-step t , which in practice are approximated via the use of a replay buffer \mathcal{D} . When sampling h_t , the state s_t is the first element of the history. The inequality constraint describes the maximum allowed KL distance between intermediate update and previous parametric policy, while the equality constraint simply ensures that the intermediate update represents a normalized distribution.

Subsequently, in order to render the following derivations more intuitive, we replace the expectations and explicitly use integrals. The Lagrangian $L(q, \eta, \gamma)$ can now be formulated as

$$L(q, \eta, \gamma) = \iiint p(h_t) q(a_t, o_t|h_t) Q_\phi(s_t, a_t, o_t) \mathrm{d}o_t \mathrm{d}a_t \mathrm{d}h_t \quad (13)$$

$$+ \eta \left(\epsilon_E - \iiint p(h_t) q(a_t, o_t|h_t) \log \frac{q(a_t, o_t|h_t)}{\pi_\theta(a_t, o_t|h_t)} \mathrm{d}o_t \mathrm{d}a_t \mathrm{d}h_t \right) \quad (14)$$

$$+ \gamma \left(1 - \iiint p(h_t) q(a_t, o_t|h_t) \mathrm{d}o_t \mathrm{d}a_t \mathrm{d}h_t \right). \quad (15)$$

Next to maximize the Lagrangian with respect to the primal variable q , we determine its derivative as,

$$\frac{\partial L(q, \eta, \gamma)}{\partial q} = Q_\phi(a_t, o_t, s_t) - \eta \log q(a_t, o_t|h_t) + \eta \log \pi_\theta(a_t, o_t|h_t) - \eta - \gamma.$$

In the next step, we can set the left hand side to zero and rearrange terms to obtain

$$q(a_t, o_t|h_t) = \pi_\theta(a_t, o_t|h_t) \exp \left(\frac{Q_\phi(s_t, a_t, o_t)}{\eta} \right) \exp \left(-\frac{\eta + \gamma}{\eta} \right).$$

The last exponential term represents a normalization constant for q , which we can formulate as

$$\frac{\eta + \gamma}{\eta} = \log \left(\iint \pi_\theta(a_t, o_t|h_t) \exp \left(\frac{Q_\phi(s_t, a_t, o_t)}{\eta} \right) \mathrm{d}o_t \mathrm{d}a_t \right). \quad (16)$$

In order to obtain the dual function $g(\eta)$, we insert the solution for the primal variable into the Lagrangian in Equation 13 which yields

$$\begin{aligned}
L(q, \eta, \gamma) &= \iiint p(h_t) q(a_t, o_t|h_t) Q_\phi(s_t, a_t, o_t) \mathrm{d}o_t \mathrm{d}a_t \mathrm{d}h_t \\
&+ \eta \left(\epsilon_E - \iiint p(h_t) q(a_t, o_t|h_t) \log \frac{\pi_\theta(a_t, o_t|h_t) \exp \left(\frac{Q_\phi(s_t, a_t, o_t)}{\eta} \right) \exp \left(-\frac{\eta + \gamma}{\eta} \right)}{\pi_\theta(a_t, o_t|h_t)} \mathrm{d}o_t \mathrm{d}a_t \mathrm{d}h_t \right) \\
&+ \gamma \left(1 - \iiint p(h_t) q(a_t, o_t|h_t) \mathrm{d}o_t \mathrm{d}a_t \mathrm{d}h_t \right).
\end{aligned}$$

We expand the equation and rearrange to obtain

$$\begin{aligned}
L(q, \eta, \gamma) &= \iiint p(h_t)q(a_t, o_t|h_t)Q_\phi(s_t, a_t, o_t) do_t da_t dh_t \\
&\quad - \eta \iiint p(h_t)q(a_t, o_t|h_t) \left[\frac{Q_\phi(s_t, a_t, o_t)}{\eta} + \log \pi_\theta(a_t, o_t|h_t) - \frac{\eta + \gamma}{\eta} \right] do_t da_t dh_t \\
&\quad + \eta \epsilon_E + \eta \iiint p(h_t)q(a_t, o_t|h_t) \log \pi_\theta(a_t, o_t|h_t) do_t da_t dh_t \\
&\quad + \gamma \left(1 - \iiint p(h_t)q(a_t, o_t|h_t) do_t da_t dh_t \right).
\end{aligned}$$

In the next step, most of the terms cancel out and after additional rearranging of the terms we obtain

$$L(q, \eta, \gamma) = \eta \epsilon_E + \eta \int p(h_t) \frac{\eta + \gamma}{\eta} dh_t.$$

We have already calculated the term inside the integral in Equation 16, which we now insert to obtain

$$\begin{aligned}
g(\eta) &= \min_q L(q, \eta, \gamma) \\
&= \eta \epsilon_E + \eta \int p(h_t) \log \left(\iint \pi_\theta(a_t, o_t|h_t) \exp \left(\frac{Q_\phi(s_t, a_t, o_t)}{\eta} \right) do_t da_t \right) dh_t \\
&= \eta \epsilon_E + \eta \mathbb{E}_{h_t \sim p(h_t)} \left[\log \left(\mathbb{E}_{a_t, o_t \sim \pi_\theta} \left[\exp \left(\frac{Q_\phi(s_t, a_t, o_t)}{\eta} \right) \right] \right) \right], \tag{17}
\end{aligned}$$

The dual in Equation 17 can finally be minimized with respect to η based on samples from the replay buffer and policy.

C.2 Parametric Option Policy Update

After obtaining the non-parametric policy improvement, we can align the parametric option policy to the current non-parametric policy. As the non-parametric policy is represented by a set of samples from the parametric policy with additional weighting, this step effectively employs a type of critic-weighted maximum likelihood estimation. In addition, we introduce regularization based on a distance function \mathcal{T} which has a trust-region effect for the update and stabilizes learning.

$$\begin{aligned}
\theta_{new} &= \arg \min_{\theta} \mathbb{E}_{h_t \sim p(h_t)} \left[\text{KL}(q(a_t, o_t|h_t) \| \pi_\theta(a_t, o_t|h_t)) \right] \\
&= \arg \min_{\theta} \mathbb{E}_{h_t \sim p(h_t)} \left[\mathbb{E}_{a_t, o_t \sim q} \left[\log q(a_t, o_t|h_t) - \log \pi_\theta(a_t, o_t|h_t) \right] \right] \\
&= \arg \max_{\theta} \mathbb{E}_{h_t \sim p(h_t), a_t, o_t \sim q} \left[\log \pi_\theta(a_t, o_t|h_t) \right], \\
\text{s.t. } &\mathbb{E}_{h_t \sim p(h_t)} \left[\mathcal{T}(\pi_{\theta_{new}}(\cdot|h_t) | \pi_\theta(\cdot|h_t)) \right] < \epsilon_M,
\end{aligned}$$

where $h_t \sim p(h_t)$ is a trajectory segment, which in practice sampled from the dataset \mathcal{D} , \mathcal{T} is an arbitrary distance function between the new policy and the previous policy. ϵ_M denotes the allowed change for the policy. We again employ Lagrangian Relaxation to enable gradient based optimization of the objective, yielding the following primal:

$$\begin{aligned}
\max_{\theta} \min_{\alpha > 0} L(\theta, \alpha) &= \mathbb{E}_{h_t \sim p(h_t), a_t, o_t \sim q} \left[\log \pi_\theta(a_t, o_t|h_t) \right] + \\
&\quad \alpha \left(\epsilon_M - \mathbb{E}_{h_t \sim p(h_t)} \left[\mathcal{T}(\pi_{\theta_{new}}(\cdot|h_t), \pi_\theta(\cdot|h_t)) \right] \right). \tag{18}
\end{aligned}$$

We can solve for θ by iterating the inner and outer optimization programs independently. In practice we find that it is most efficient to update both in parallel.

We also define the following distance function between old and new option policies

$$\mathcal{T}(\pi_{\theta_{new}}(\cdot|h_t), \pi_{\theta}(\cdot|h_t)) = \mathcal{T}_H(h_t) + \mathcal{T}_T(h_t) + \mathcal{T}_L(h_t)$$

$$\mathcal{T}_H(h_t) = \text{KL}(\text{Cat}(\{\alpha_{\theta_{new}}^j(h_t)\}_{j=1\dots M}) \parallel \text{Cat}(\{\alpha_{\theta}^j(h_t)\}_{j=1\dots M}))$$

$$\mathcal{T}_T(h_t) = \frac{1}{M} \sum_{j=1}^M \text{KL}(\text{Cat}(\{\beta_{\theta_{new}}^{ij}(h_t)\}_{j=1\dots 2}) \parallel \text{Cat}(\{\beta_{\theta}^{ij}(h_t)\}_{j=1\dots 2}))$$

$$\mathcal{T}_L(h_t) = \frac{1}{M} \sum_{j=1}^M \text{KL}(\mathcal{N}(\mu_{\theta_{new}}^j(h_t), \Sigma_{\theta_{new}}^j(h_t)) \parallel \mathcal{N}(\mu_{\theta}^j(h_t), \Sigma_{\theta}^j(h_t)))$$

where \mathcal{T}_H evaluates the KL between the categorical distributions of the high-level controller, \mathcal{T}_T is the average KL between the categorical distributions of the all termination conditions, and \mathcal{T}_L corresponds to the average KL across Gaussian components. In practice, we can exert additional control over the convergence of model components by applying different ϵ_M to different model parts (high-level controller, termination conditions, options).

C.3 Transition Probabilities for Option and Switch Indices

The transitions for option o and switch index n are given by:

$$p(o_t, n_t | s_t, o_{t-1}, n_{t-1}) = \begin{cases} (1 - \beta(s_t, o_{t-1})) & \text{if } n_t = n_{t-1}, o_t = o_{t-1} \\ \beta(s_t, o_{t-1}) \pi^C(o_t | s_t) & \text{if } n_t = n_{t-1} + 1 \\ 0 & \text{otherwise} \end{cases} \quad (19)$$